J. Fluid Mech. (2010), *vol.* 662, *pp.* 123–133.
doi:10.1017/S0022112010003885

A numerical study of the effect of fibre stiffness on the rheology of sheared flexible fibre suspensions

JINGSHU WU AND CYRUS K. AIDUN†

G. W. Woodruff School of Mechanical Engineering, Georgia Institute of Technology, 500 10th Street NW, Atlanta, GA 30332, USA

(Received 14 February 2010; revised 13 July 2010; accepted 13 July 2010; first published online 27 September 2010)

A recently developed particle-level numerical method is used to simulate flexible fibre suspensions in Newtonian simple shear flow. In this method, the flow is computed on a fixed regular 'lattice' using the lattice Boltzmann method, where each solid particle, or fibre in this case, is mapped onto a Lagrangian frame moving continuously through the domain. The motion and orientation of the fibre are obtained from Newtonian dynamics equations. The effect of fibre stiffness on the rheology of flexible fibre suspensions is investigated and a relation for the relative viscosity is obtained. We show that fibre stiffness (bending ratio, BR) has a strong impact on rheology in the range $BR < 3$. The relative viscosity increases significantly as BR decreases. These results show that the primary normal stress difference has a minimum value at $BR \sim 1$. The primary normal stress difference for slightly deformable fibres reaches a minimum and increases significantly as BR decreases below one. The results are explained based on Batchelor's relation for non-Brownian suspensions.

Key words: rheology, slender-body theory, suspensions

1. Introduction

Fibre stiffness plays an important role in determining the rheological properties of fibre suspensions. It is known that the microstructure and rheology of fibre suspensions depend on fibre volume fraction, aspect ratio and flexibility. Most previous theoretical and experimental studies are focused on the first two factors. Hence an understanding of the effect of fibre stiffness on the microstructure and rheology of flexible fibre suspensions is of both practical and theoretical interest. In this paper, we employ a particle-level simulation method to understand the underlying physical processes. The dynamics of each fibre are solved numerically to calculate the fibre's position and orientation and thus to predict the fibre suspension's microstructure. The rheological properties are computed based on direct numerical simulation of fibre suspensions.

Claeys & Brady (1993) have done extensive numerical calculations for elongated particles in an unbounded fluid with hydrodynamic interactions using Stokesian dynamics. Yamane, Kaneda & Doi (1994) and Fan, Phan-Thien & Zheng (1998) included both long-range hydrodynamic interactions and lubrication resistance force in their simulations. These authors obtained good agreement with early experiments

† Email address for correspondence: cyrus.aidun@me.gatech.edu

by Carter (1967), Goto, Nagazono & Kato (1986), Bibbo, Dinh & Armstrong (1985) and Stover, Koch & Cohen (1992).

In all the above mentioned studies, the fibre is considered as a rigid rod-like cylinder in Stokes flow where the inertia of fluid and fibre is ignored. Experimental studies (Forgacs & Mason 1959; Blakeney 1966; Goto *et al.* 1986) have shown that slight fibre curvature would change the period of fibre rotation and the shear viscosity of the suspension. If the fibre's geometry is important, then the fibre's flexibility is equally important. Yamamoto & Matsuoka (1992) modelled a flexible fibre as a chain of spring-linked spheres. The constraints for springs are implemented in the equation of motion. Joung, Phan-Thien & Fan (2001) followed a similar idea and used 'spring-linked spheres' to model long flexible fibres. The relative viscosities for fibres having different flexibility were calculated and compared with experimental results from Bibbo (1987).

Ross & Klingenberg (1997) treated a flexible fibre as a chain of rigid prolate spheroids connected by ball and socket joints. Compared to Yamamoto & Matsuoka's model, there is no need to solve the iterative constraints for connected springs, and the model can extend to high-aspect-ratio fibres. Schmid, Switzer & Klingenberg (2000) followed this idea and modelled flexible fibres as chains of rigid rods. Their research focused on fibre flocculation, and they concluded that flocculation is strongly affected by interparticle forces and fibre deformations. However, they did not consider the hydrodynamic interactions between fibres, nor the two-way coupling between fibres and the suspending fluid. Lindstrom & Uesaka (2008) did similar investigations by using the same model to simulate flexible fibres with high aspect ratio. These researchers demonstrated that fibre concentration, aspect ratio, equilibrium geometry, fibre flexibility and fibre–fibre interactions are important factors in determining the suspension microstructure and rheology.

In this study, we use the recently developed particle-level numerical method (Wu & Aidun 2010*a*) combined with the lattice-Boltzmann fluid-phase solver (Aidun, Lu & Ding 1998) to obtain the microstructure and rheological properties of flexible fibre suspensions. The important aspects of this study are (i) simulations include mechanical fibre–fibre interactions and lubrication forces, (ii) the fluid and fibres are two-way coupled with direct numerical simulation, (iii) the physical properties of the flexible fibre are directly related to simulation parameters and (iv) the present method can efficiently simulate large numbers of flexible fibres (of the order of 10^4) in a periodic cell with the range of simulation extended to a concentrated regime of industrial interest, beyond the range of the earlier studies. In this study, the motion and orientation of the fibre are obtained from Newtonian dynamics equations. The fibre deformation is calculated by an efficient flexible fibre model. The no-slip boundary condition at the fluid–solid interface is based on the external boundary force (EBF) method. The details of this method are presented in previous papers (Wu & Aidun 2010*a*,*b*). Detailed explanation and derivation of the methodology can be found in these two papers.

The remainder of this paper is organized as follows. In § 2, fibre-suspension rheology and the related parameters are described in detail. Results from several simulations with various fibre stiffness, aspect ratio and volume concentration are presented in § 3. Some physical explanations and discussions are also included in this section, with some concluding remarks in § 4.

2. Fibre-suspension rheology

To classify the level of fibre concentration, this study follows the classification of fibre concentration by Doi & Edwards (1978) based on the value of nL^3, where n is

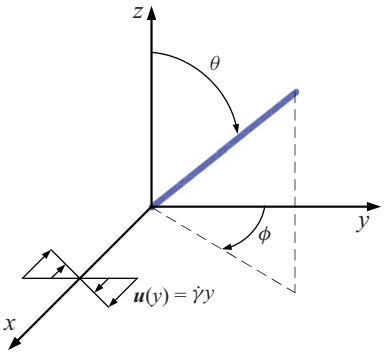

FIGURE 1. (Colour online) The spherical coordinate system for a fibre in an x, y simple shear flow.

the number of fibres per unit volume and L is the fibre length. In the dilute regime when $nL^3 < 1$, the fibres move without interference from other fibres. In the semi-dilute regime, $1 < nL^3 < L/D$, where D is the fibre diameter, some fibre contacts are possible. In the concentrated regime, $nL^3 > L/D$, fibre–fibre interaction is dominant. The fibre-suspension parameters of relevance in this study are the fibre aspect ratio ($r_p = L/D$), fibre volume fraction ($c_{vf} = nL\pi D^2/4$) and fibre bending ratio (BR), which is the non-dimensional measure of fibre stiffness. The bending ratio is defined by Forgacs & Mason (1959) and Goldsmith & Mason (1967) as

$$BR \equiv \frac{E_Y(\ln 2r_e - 1.5)}{2(\mu\dot{\gamma})r_p^4}. \tag{2.1}$$

Here, E_Y is the fibre Young's modulus, μ is the fluid viscosity, $\dot{\gamma}$ is the shear rate and r_e is the effective aspect ratio. For a rigid cylinder of aspect ratio $r_p = L/D$, $r_e = 1.24r_p/\sqrt{\ln r_p}$ (Cox 1971). For an axisymmetric slender particle in the Stokes flow, the governing equations are given by Jeffery (1922)

$$\tan\phi = r_e \tan\left(\frac{2\pi t}{T_p} + \phi_0\right), \tag{2.2}$$

$$\tan\theta = \frac{C_j r_e}{\left(r_e^2\cos^2\phi + \sin^2\phi\right)^{1/2}}, \tag{2.3}$$

where ϕ and θ are the orientation angles as shown in figure 1. C_j and ϕ_0 are the Jeffery orbit constant and phase angle, respectively. It is advantageous to use $C_b \equiv C_j/(C_j + 1)$, since C_j takes values from 0 to ∞, while C_b is bound between 0 and 1.

In this study, the Péclet number $Pe \sim 10^{14}$, so Brownian motion is negligible. The particle Reynolds number, $Re = \dot{\gamma}LD/\nu$, is very small (1.72×10^{-5} to 5.59×10^{-5}) and therefore inertia is negligible.

The rheological properties presented below are directly computed based on numerical computation of the averaged stress tensor in a cubic-box-shaped subdomain within an unbounded computational shear domain based on the Lees–Edwards boundary condition. The details of the computational method are outlined in Wu & Aidun (2010*a*). The relative shear viscosity η is given by

$$\eta \equiv \frac{\mu_{eff}}{\mu} = \frac{\sigma_{xy}}{2\mu E_{xy}}, \tag{2.4}$$

where μ_{eff} is the effective shear viscosity, μ is the viscosity of the suspending fluid, $E_{xy} = \dot{\gamma}/2$ is the shear strain component of the strain rate tensor, $\boldsymbol{E}$, and σ_{xy} is the

shear stress component of the stress tensor, $\boldsymbol{\sigma}$. The first normal stress difference is given by

$$N_1 \equiv \sigma_{xx} - \sigma_{yy}. \tag{2.5}$$

The Batchelor's relation (Batchelor 1971) for the contribution of the suspended fibres to the stress tensor in dilute suspensions without Brownian motion would be useful in explaining some of the computational results. This relation is given by

$$\boldsymbol{\sigma}^B = 2\mu \boldsymbol{E} + \mu_{fibre}\left(\langle \boldsymbol{pppp}\rangle - \tfrac{1}{3}\boldsymbol{I}_n\langle \boldsymbol{pp}\rangle\right) : \boldsymbol{E}, \tag{2.6}$$

where $\boldsymbol{I}_n$ is the unit tensor, $\boldsymbol{p} = p_x\boldsymbol{e_x} + p_y\boldsymbol{e_y} + p_z\boldsymbol{e_z}$ is a unit vector parallel to the fibre axis of symmetry and $\boldsymbol{e_x}$, $\boldsymbol{e_y}$ and $\boldsymbol{e_z}$ are the unit vectors in the flow direction, velocity gradient direction and vorticity axis direction, respectively. The angle bracket, $\langle\rangle$, represents an average over all the suspended fibres. μ_{fibre} is a function of fibre concentration, orientation distribution and fibre aspect ratio. From (2.6), it can be shown that the relative viscosity, η^B, is given by

$$\eta^B = \frac{\sigma^B_{xy}}{2\mu E_{xy}} = 1 + \frac{\mu_{fibre}}{\mu}\langle p_x^2 p_y^2\rangle, \tag{2.7}$$

and the first effective normal stress difference is given by

$$N_1^B = \sigma^B_{xx} - \sigma^B_{yy} = \mu_{fibre}\dot{\gamma}\left(\langle p_x^3 p_y\rangle - \langle p_y^3 p_x\rangle\right). \tag{2.8}$$

The rheological properties calculated from (2.7) and (2.8) depend on the accuracy of Batchelor's theory which requires that fibres move freely with no fibre–fibre interactions. In this study, we investigate suspensions from dilute to concentrated regimes, where all rheological properties are calculated directly from computational results without such restriction. Here Batchelor's theory is presented only to explain the relation between the fibre-orientation distribution and the pure hydrodynamic contribution to the suspension stress. This feature is very helpful in explaining the results in § 3.

Both the relative shear viscosity and effective normal stress differences are important in describing the non-Newtonian nature of fibre suspensions. The effective normal stress difference shows the non-symmetric changes in the $p(\phi)$ distribution function. The moments in (2.5) are all zero if the orientation distribution function is symmetric with respect to the xz-plane. These moments are very small and sensitive, and they are difficult to measure by experimental techniques. Bibbo (1987) confirmed that the transient normal stress difference was proportional to $\dot{\gamma}$, but the value of the normal force was below the sensitivity of the rheometer.

3. Results and discussion

Validation of the lattice Boltzmann approach with the EBF method for fibre suspensions and details of the computational method are presented in previous publications (Wu & Aidun 2010*a*,*b*) and will not be repeated here. The focus of this study is to investigate the effect of fibre stiffness on the rheology of flexible fibre suspensions. Fibres with different stiffness, aspect ratio and volume concentration are considered.

An unbounded shear domain is implemented based on the Lees–Edwards boundary condition (Lees & Edwards 1972), as described by Wagner & Pagonabarraga (2002) and MacMeccan *et al.* (2009), to improve computational efficiency and to remove wall effects. All simulations are in lattice Boltzmann (LB) units where the computational domain is $4L \times 5L \times 4L$, the fibre diameter is 0.4 lattice units, density is 1, viscosity is

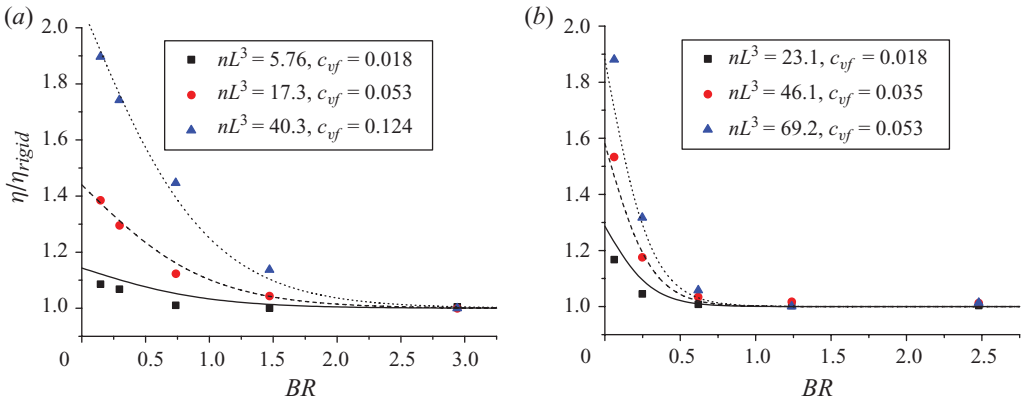

FIGURE 2. (Colour online) Normalized relative viscosity, η/η_{rigid}, versus fibre-bending ratio, BR, for flexible fibre suspensions with different fibre aspect ratio, r_p, and volume concentration c_{vf}. η is the relative viscosity of the flexible fibre suspension and η_{rigid} is the relative viscosity of the rigid fibre suspension with the same r_p and c_{vf}. The solid line (–), dashed line (- - -) and dotted line (···) are the corresponding curve-fitting results. (a) $r_p = 16$ and (b) $r_p = 32$.

1/6, and the shear rate is 1.12×10^{-6} corresponding to $Re = 1.72 \times 10^{-5}$ for $r_p = 16$. The values in the physical units depend on the fluid properties. For example, for PDMS10k used by Bibbo (1987), where the dynamic viscosity is 13 Pa s, the density is 0.97×10^3 kg m^{-3} and fibre diameter 0.12 mm, the shear rate of 1 s^{-1} gives the same value of $Re = 1.72 \times 10^{-5}$.

3.1. *Relative viscosity*

To study the effect of fibre stiffness on relative viscosity, two cases with aspect ratio $r_p = 16$ and 32 are considered. Figure 2 shows that the fibre bending ratio, BR, at a given shear rate, has a significant influence on the suspension's relative viscosity. In all of the results presented here, shear rate remains constant where BR changes by changing the Young's modulus. When $BR < 3$, the suspension viscosity is indeed inversely related to the fibre stiffness, while for $BR > 3$, the fibre can be considered as rigid. The difference between flexible fibres and rigid fibres is quite large. For fibres with the same aspect ratio, this difference increases as suspension concentration increases. The difference also increases with fibre aspect ratio for suspensions having the same concentration. It should be emphasized that BR should be considered as a non-dimensional measure of fibre deformation. Variation in shear rate will influence fibre deformation as well as fibre–fibre interaction, and both effects influence the rheological properties. In other words, relative viscosity is a function of $\dot{\gamma}$ as well as BR. Hence, all results shown here are particular to the shear rate of 1.12×10^{-6} in LB units, though similar trends with BR are expected at other rates of shear.

The relative viscosity of a flexible fibre suspension may be fitted with the empirical equation (Joung *et al.* 2001),

$$\eta = \eta_{rigid}\left(1 + \frac{A0}{1 + \mathrm{e}^{BR/A1}}\right). \tag{3.1}$$

Here $A0$ and $A1$ are parameters that can be determined from the simulation data by least-squares curve fitting. From the simulation results, these two parameters are estimated to be

$$A0 = r_p(1.00082c_{vf} + 0.69672c_{vf}^2), \quad A1 = 70/r_e^2. \tag{3.2}$$

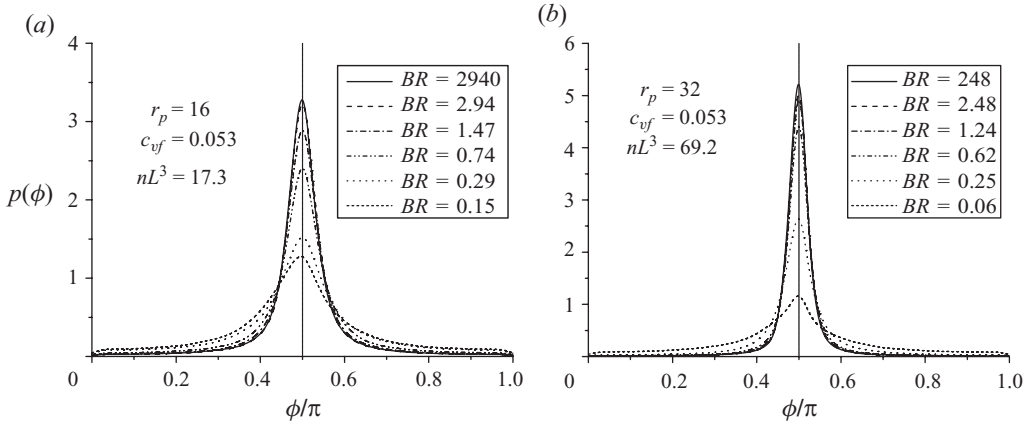

FIGURE 3. The ϕ distribution for flexible fibre suspensions with different aspect ratio r_p and bending ratio BR. Fibre volume fraction $c_{vf} = 0.053$.

Equation (3.1) is then used to fit the simulation data, as shown in figure 2. This relation can be used to predict the flexible fibre suspension viscosity. The relative viscosity of a rigid fibre suspension can be easily found through existing methods; one only needs to know the fibre bending ratio BR, fibre aspect ratio r_p and the suspension volume fraction c_{vf} to find the two parameters in (3.2) and then calculate the relative viscosity for the flexible fibre suspension using (3.1).

The effect of fibre stiffness (BR) on the relative viscosity can be explained based on the fibre-orientation distribution. The relation based on Batchelor's theory is presented here. This equation is in principle valid only in the dilute regime. However, Batchelor's theory clearly relates rheological properties with suspension microstructure, including the effects of hydrodynamic interactions. The equations are based on the fibre-orientation distribution, implicitly including some of the effects of non-hydrodynamic interactions.

Based on the spherical coordinate system, as shown in figure 1, (2.7) becomes

$$\eta^B = 1 + \frac{\mu_{fibre}}{\mu} \langle p_x^2 p_y^2 \rangle = 1 + \frac{\mu_{fibre}}{4\mu} \langle \sin^4\theta \sin^2 2\phi \rangle. \tag{3.3}$$

Equation (3.3) shows that the fibre orientation has a strong influence on the suspension's shear viscosity. The shear stress has a maximum value when the fibre-orientation angle ϕ is equal to $\pi/4$ or $3\pi/4$ and has a minimum value when ϕ is equal to 0, $\pi/2$ or π.

Figure 3 shows the ϕ distribution, with different aspect ratio and bending ratio BR for suspensions with fibre volume fraction $c_{vf} = 0.053$. For suspensions with the same volume fraction and fibre aspect ratio, at lower bending ratio (i.e. more flexible), the ϕ distribution becomes broader with a lower peak, showing that the suspending fibres are mostly oriented away from the xz-plane, thus increasing the suspension shear viscosity. Also the asymmetry of the ϕ distribution, observed in the small BR range, indicates that the fibre–fibre mechanical interaction and fibre deformation are present in this regime. The consequences of this observation will be discussed further below.

3.2. *First normal stress difference*

In this section the dependence of the first normal stress difference N_1 on the fibre stiffness BR and fibre volume fraction c_{vf} is investigated. First, the simulation results are compared with experimental results from the literature as shown in figure 4.

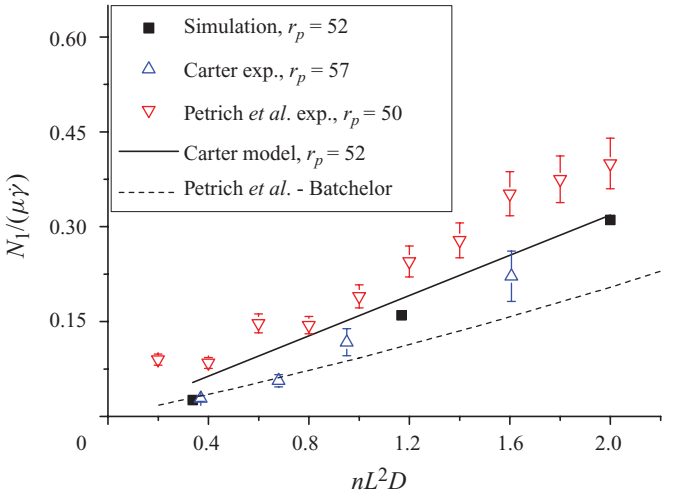

FIGURE 4. (Colour online) The non-dimensional first normal stress difference $N_1/(\mu\dot{\gamma})$ as a function of nL^2D for rigid fibre suspensions. The open triangles (△) are the experimental data of Carter (1967) and the open upside-down triangles (▽) are the experimental data of Petrich *et al.* (2000). The solid line (—) is the prediction of Carter's model, (3.5), with $K_c = 0.08$. The dashed line (- - -) is the Batchelor's first normal stress difference N_1^B, (2.8), calculated by Petrich *et al.* (2000). The solid squares (■) are the simulation results from the present lattice-Boltzmann method with EBF.

Petrich, Koch & Cohen (2000) and Carter (1967) performed experiments in semi-dilute and concentrated regimes with results showing similar patterns with some discrepancy. Petrich *et al*. also measured the average value of $(\langle p_x^3 p_y\rangle - \langle p_y^3 p_x\rangle)$ and calculated the Batchelor's first normal stress difference N_1^B by using (2.8), as shown in figure 4. The value of N_1^B computed by Petrich *et al*. (2000) is much lower than the experimental result. The discrepancy increases with fibre concentration. As previously discussed, Batchelor's theory only includes hydrodynamic contributions, but in the semi-dilute and concentrated regimes, non-hydrodynamic interactions and fibre–fibre interacions become important. Present simulation results are closer to Carter's experimental results with the same discrepancy compared to Batchelor's solutions.

Based on the following relation, Carter (1967) predicts the first normal stress difference for rigid fibre suspensions to be given by

$$\frac{N_1^C}{\mu\dot{\gamma}} \propto \frac{c_{vf} r_p^2}{\ln(2r_p) - 1.8} \langle \sin(2\phi)\rangle. \tag{3.4}$$

Carter assumes that $\langle \sin(2\phi)\rangle \propto \sqrt{1/r_p}$, and therefore (3.4) can be written as

$$\frac{N_1^C}{\mu\dot{\gamma}} = K_c \frac{c_{vf} r_p^{3/2}}{\ln(2r_p) - 1.8}, \tag{3.5}$$

where K_c is a constant to be determined experimentally. Different investigators applied Carter's model to their normal stress measurements (Carter 1967; Kitano & Kataoka 1981; Goto *et al.* 1986; Zirnsak, Hur & Boger 1994; Petrich *et al.* 2000; Sepehr *et al.* 2004; Keshtkar, Heuzey & Carreau 2009). The measured data fall within a range for K_c from 0.04 to 0.32, although no clear relation between K_c and variables such as fibre volume fraction and aspect ratio has been reported. We also

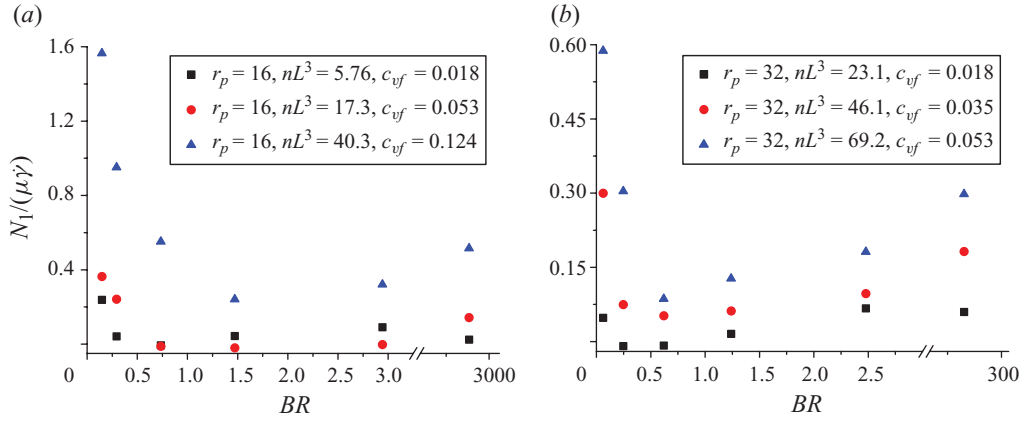

FIGURE 5. (Colour online) The non-dimensional first normal stress difference $N_1/(\mu\dot{\gamma})$ versus fibre bending ratio, BR, for flexible fibre suspensions with different fibre aspect ratio r_p and volume concentration c_{vf}.

implemented Carter's formula with our simulation results using $K_c = 0.08$, the same as Petrich *et al.* (2000) ($K_c = 0.08$) and similar to Keshtkar *et al.* (2009) ($K_c = 0.1 \pm 0.01$) in their studies, as shown with the solid line in figure 4. The Carter's model predicts the trend of the experimental results, not the value, by choosing the appropriate K_c. According to Lindstrom & Uesaka (2008), the assumption for the model, $\langle \sin(2\phi) \rangle \propto \sqrt{1/r_p}$, becomes more valid in a concentrated regime.

Figure 5 shows the effect of fibre flexibility on the non-dimensional fibre normal stress difference for fibres with aspect ratio $r_p = 16$ and 32. These results show that an increase in fibre volume fraction leads to an increase of the first normal stress difference. Higher volume fraction results in more fibre–fibre interaction and consequently increases N_1. It is interesting to note that for suspensions with the same fibre volume fraction, the first normal stress difference will decrease with decreasing bending ratio reaching a minimum at a critical bending ratio BR_c close to one, and will then increase with decreasing BR below BR_c. A similar trend is also found in the experimental data of Keshtkar *et al.* (2009). It is apparent that the suspension parameters such as fibre aspect ratio, fibre stiffness, volume concentration and suspension microstructure can influence N_1. However, it is interesting to see if the trend observed in figure 5 can be explained using Batchelor's theory. Based on the spherical coordinate system, as shown in figure 1, (2.8) becomes

$$N_1^B = \mu_{fibre}\dot{\gamma}\left(\langle p_x^3 p_y \rangle - \langle p_y^3 p_x \rangle\right) = -\frac{\mu_{fibre}\dot{\gamma}}{4}\left(\langle \sin^4\theta \sin 4\phi \rangle\right). \tag{3.6}$$

Equation (3.6) shows that in the absence of direct physical contact between fibres and without fibre deformation (rigid fibre), the fibre-orientation distribution $p(\phi)$ would be symmetric about the xz-plane; therefore, $N_1^B = 0$, since it is an odd function of p_y. In other words, if direct contact between fibres exists or if fibres are deformable, N_1^B will not vanish. Figure 3 shows that for decreasing bending ratio, BR (more flexible fibre), the mean orientation angle $\langle \phi \rangle$ becomes slightly less than $\pi/2$, $\langle \sin 4\phi \rangle$ becomes a small negative value. This small asymmetry of the fibre-orientation distribution gives rise to a positive value of N_1^B based on (3.6).

On the other hand, the orientation distribution of θ is also very important for the first normal stress difference, as shown in (3.6). N_1^B increases with θ, where θ is

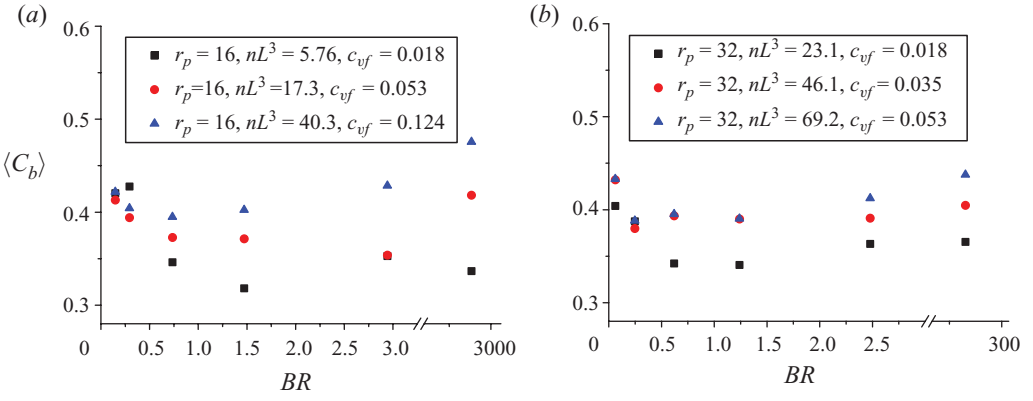

FIGURE 6. (Colour online) The mean orbit constant $\langle C_b \rangle$ versus fibre bending ratio, BR, for flexible fibre suspensions with different fibre aspect ratio r_p and volume concentration c_{vf}.

directly related to the orbit constant C_b, and C_b can be calculated numerically for every fibre with (2.3). Figure 6 shows the relation between the mean orbit constant $\langle C_b \rangle$ and the fibre bending ratio. Based on bending ratio BR and (3.6), the relation between θ, $p(\phi)$ and N_1^B can be divided into two regimes (BR less than or greater than BR_c). When $BR > BR_c$, the suspending fibres are rigid or slightly deformable. The suspensions have similar fibre-orientation distribution, $p(\phi)$, as shown in figure 3 and the orientation angle θ is the main factor for changing N_1^B. Decreasing BR reduces the orientation angle θ and the mean orbit constant $\langle C_b \rangle$. N_1^B decreases with decreasing BR. When $BR < BR_c$, the suspended fibres become flexible. Both θ and $p(\phi)$ become important factors for N_1^B. In this regime, the suspending fibres are more randomly oriented and $\langle C_b \rangle$ increases with decreasing bending ratio, $\langle C_b \rangle \sim 0.45$ when $BR \to 0$. At the same time, the fibre-orientation distribution $p(\phi)$ becomes more asymmetric and N_1^B increases with decreasing BR.

It is important to note that (3.6) only includes the hydrodynamic contributions from the suspension, and does not include non-hydrodynamic interactions and fibre–fibre interactions. Therefore, the first normal stress difference, shown in figure 5, is not strictly proportional to the orbit constant C_b in figure 6, even if they have the same fibre-orientation distribution $p(\phi)$.

4. Conclusion

The direct computational method developed by Wu & Aidun (2010*a*,*b*) for fibre suspensions has been useful for analysis of the rheology of flexible fibre suspensions in unbounded shear. In particular, the ability to directly compute the fibre-orientation distribution allows better insight into the effect of fibre flexibility on effective viscosity and first normal stress difference investigated in this study. As fibre flexibility increases (i.e. BR decreases), the relative suspension viscosity increases significantly. This is due to broader fibre-orientation distribution in the vorticity plane based on fibre deformation and increase in fibre–fibre interaction. As bending ratio decreases, fibre deformations in the compression and extension axes vary resulting in an asymmetric fibre orientation distribution $p(\phi)$. It is shown that asymmetry in $p(\phi)$ either due to fibre deformation or direct fibre–fibre contact results in positive primary normal stress difference.

REFERENCES

Aidun, C. K., Lu, Y. & Ding, E. 1998 Direct analysis of particulate suspensions with inertia using the discrete Boltzmann equation. *J. Fluid Mech.* **373**, 287–311.

Batchelor, G. K. 1971 The stress generated in a non-dilute suspensions of elongated particles by pure straining motion. *J. Fluid Mech.* **46**, 813–829.

Bibbo, M. A. 1987 Rheology of semi-concentrated fiber suspensions. PhD thesis, Massachusetts Institute of Technology, Cambridge, MA.

Bibbo, M. A., Dinh, S. M. & Armstrong, R. C. 1985 Shear flow properties of semi-concentrated fibre suspensions. *J. Rheol.* **29**, 905–929.

Blakeney, W. R. 1966 The viscosity of suspensions of straight, rigid rods. *J. Colloid Interface Sci.* **22**, 324–330.

Carter, L. F. 1967 A study of the rheology of suspensions of rod-shaped particles in a Navier–Stokes liquid. PhD thesis, University of Michigan, Ann Arbor, MI.

Claeys, I. L. & Brady, J. F. 1993 Suspensions of prolate spheroids in Stokes flow. Part 1. Dynamics of a finite number of particles in an unbounded fluid. *J. Fluid Mech.* **251**, 411–442.

Cox, R. G. 1971 The motion of long slender bodies in a viscous fluid. Part 2. Shear flow. *J. Fluid Mech.* **45**, 625–657.

Doi, M. & Edwards, S. F. 1978 Dynamics of concentrated polymer systems. Part I. Brownian motion in equilibrim state. *J. Chem. Soc. Faraday Trans.* II **74**, 1789–1801.

Fan, X., Phan-Thien, N. & Zheng, R. 1998 A direct simulation of fibre suspensions. *J. Non-Newtonian Fluid Mech.* **74**, 113–135.

Forgacs, O. L. & Mason, S. G. 1959 Particle motions in sheared suspensions. Part 9. Spin and deformation of thread-like particles. *J. Colloid Interface Sci.* **14**, 457–472.

Goldsmith, H. L. & Mason, S. G. 1967 The microrheology of dispersions. *Rheology* **4**, 85–201.

Goto, S., Nagazono, H. & Kato, H. 1986 The flow behaviour of fiber suspensions in Newtonian fluids and polymer solutions. Part I. Mechanical properties. *Rheol. Acta* **25**, 119–129.

Jeffery, G. B. 1922 The motion of ellipsoidal particles immersed in a viscous fluid. *Proc. R. Soc. Lond.* A **102**, 161–179.

Joung, C. G., Phan-Thien, N. & Fan, X. J. 2001 Direct simulation of flexible fibers. *J. Non-Newtonian Fluid Mech.* **99**, 1–36.

Keshtkar, M., Heuzey, M. C. & Carreau, P. J. 2009 Rheological behavior of fiber–filled model suspensions: Effect of fiber flexibility. *J. Rheol.* **53**, 631–650.

Kitano, T. & Kataoka, T. 1981 The rheology of suspensions of vinylon fibers in polymer liquids. Part I. Suspensions in silicone oil. *Rheol. Acta* **20**, 390–402.

Lees, A. W. & Edwards, S. F. 1972 The computer study of transport processes under extreme conditions. *J. Phys.* C **5**, 1921–1928.

Lindstrom, S. B. & Uesaka, T. 2008 Simulation of semi-dilute suspensions of non-Brownian fibers in shear flow. *J. Chem. Phys.* **128**, 024901.

MacMeccan, R. M., Clausen, J. R., Neitzel, G. P. & Aidun, C. K. 2009 Simulating deformable particle suspensions using a coupled lattice-Boltzmann and finite-element method. *J. Fluid Mech.* **618**, 13–39.

Petrich, M. P., Koch, D. L. & Cohen, C. 2000 An experimental determination of the stress-microstructure relationship in semi-concentrated fiber suspensions. *J. Non-Newtonian Fluid Mech.* **95**, 101–133.

Ross, R. F. & Klingenberg, D. J. 1997 Dynamic simulation of flexible fibers composed of linked rigid bodies. *J. Chem. Phys.* **106**, 2949–2960.

Schmid, C. F., Switzer, L. H. & Klingenberg, D. J. 2000 Simulation of fiber flocculation: effects of fiber properties and interfiber friction. *J. Rheol.* **44**, 781–809.

Sepehr, M., Carreau, P. J., Moan, M. & Ausias, G. 2004 Rheological properties of short fiber model suspensions. *J. Rheol.* **48**, 1023–1048.

Stover, C. A., Koch, D. L. & Cohen, C. 1992 Observations of fiber orientation in simple shear flow of semi-dilute suspensions. *J. Fluid Mech.* **238**, 277–296.

Wagner, A. J. & Pagonabarraga, I. 2002 Lees–Edwards boundary conditions for lattice Boltzmann. *J. Stat. Phys.* **107**, 521–537.

Wu, J. & Aidun, C. K. 2010*a* A method for direct simulation of flexible fiber suspensions using lattice-Boltzmann equation with external boundary force. *Intl J. Multiphase Flow* **36**, 202–209.

Wu, J. & Aidun, C. K. 2010*b* Simulating 3d deformable particle suspensions using lattice B oltzmann method with discrete external boundary force. *Intl J. Numer. Method Fluids* **62**, 765–783.

Yamamoto, S. & Matsuoka, T. 1992 A method for dynamic simulation of rigid and flexible fibers in a flow field. *J. Chem. Phys.* **98**, 644–650.

Yamane, Y., Kaneda, Y. & Doi, M. 1994 Numerical simulation of semi-dilute suspensions of rod-like particles in shear flow. *J. Non-Newtonian Fluid Mech.* **54**, 405–421.

Zirnsak, M. A., Hur, D. U. & Boger, D. V. 1994 Normal stresses in fibre suspensions. *J. Non-Newtonian Fluid Mech.* **54**, 153–193.